Spectral properties of whistler-mode waves in the vicinity of the Moon: A statistical study with ARTEMIS

Wataru Sawaguchi[1], Yuki Harada[1], Satoshi Kurita[1], and Satoko Nakamura[2]

[1]Kyoto University
[2]Institute for Space-Earth Environmental Research

November 24, 2022

Abstract

We present statistical analyses of whistler-mode waves observed by Acceleration, Reconnection, Turbulence and Electrodynamics of the Moon's Interaction with the Sun (ARTEMIS). Although some observations showed rising tone elements of the lunar whistler-mode waves similar to the terrestrial chorus emissions, it remains unknown whether a banded structure typically seen in chorus is common to the lunar waves. In this study, we automatically detected whistler-mode waves from 9 years of ARTEMIS data and classified them into four types of spectral shapes: lower band only, upper band only, banded, and no-gap. We first show that magnetic connection to the lunar surface is a dominant factor in the wave generation; the occurrence rate of whistler mode waves is more than 10 times larger on magnetic field lines connected to the Moon than on unconnected field lines. Then we compared the field line connected events according to the position of the Moon and the condition of the field-line foot point (day/night and existence of lunar magnetic anomalies). The results show that (i) almost no banded event is observed in any circumstances, suggesting that generation mechanisms for the two band structure on the terrestrial chorus are largely ineffective around the Moon, and (ii) the wave occurrence rate depends on the foot point conditions, presumably affected by electrostatic/magnetic reflections deforming the velocity distribution of the resonant electrons. Thus, our results provide implications for the two band structure formation and new insights to fundamental processes of the Moon-plasma interaction.

Spectral properties of whistler-mode waves in the vicinity of the Moon: A statistical study with ARTEMIS

W. Sawaguchi[1], Y. Harada[1], S. Kurita[2], and S. Nakamura[3]

[1]Department of Geophysics, Graduate School of Science, Kyoto University, Kyoto, Japan.
[2]Research Institute for Sustainable Humanosphere, Kyoto University, Uji, Japan.
[3]Institute for Space-Earth Environmental Research, Nagoya University, Nagoya, Japan.

Key Points:

- We present a statistical study on Moon-related whistler-mode waves classified into 4 types of spectral shapes using ARTEMIS data
- Banded waves are extremely rare, suggesting that two band structure formation is ineffective around the Moon
- Whistler-mode wave spectra are highly variable resulting from spatial and temporal variability of the lunar plasma environment

Corresponding author: Wataru Sawaguchi, `sawag@kugi.kyoto-u.ac.jp`

Abstract

We present statistical analyses of whistler-mode waves observed by Acceleration, Reconnection, Turbulence and Electrodynamics of the Moon's Interaction with the Sun (ARTEMIS). Although some observations showed rising tone elements of the lunar whistler-mode waves similar to the terrestrial chorus emissions, it remains unknown whether a banded structure typically seen in chorus is common to the lunar waves. In this study, we automatically detected whistler-mode waves from 9 years of ARTEMIS data and classified them into four types of spectral shapes: lower band only, upper band only, banded, and no-gap. We first show that magnetic connection to the lunar surface is a dominant factor in the wave generation; the occurrence rate of whistler mode waves is more than 10 times larger on magnetic field lines connected to the Moon than on unconnected field lines. Then we compared the field line connected events according to the position of the Moon and the condition of the field-line foot point (day/night and existence of lunar magnetic anomalies). The results show that (i) almost no banded event is observed in any circumstances, suggesting that generation mechanisms for the two band structure on the terrestrial chorus are largely ineffective around the Moon, and (ii) the wave occurrence rate depends on the foot point conditions, presumably affected by electrostatic/magnetic reflections deforming the velocity distribution of the resonant electrons. Thus, our results provide implications for the two band structure formation and new insights to fundamental processes of the Moon-plasma interaction.

1 Introduction

Whistler-mode waves in space are generally electromagnetic waves excited at frequencies below the electron cyclotron frequency (f_{ce}). Here, $f_{ce} = eB/2\pi m$, where e and m are the absolute value of the electron charge and mass, respectively, and B is the background magnetic field strength. In the linear growth theory in cold plasmas (Kennel & Petschek, 1966), the excitation efficiency of whistler-mode waves depends on the temperature anisotropy and the population of resonant electrons. The excitation needs a perpendicular temperature higher than a parallel temperature and abundant hot electrons. The temperature anisotropy originates, for example, from perpendicular heating of electrons injected from the magnetotail during substorms. A well-known example of whistler-mode waves is chorus emissions that have been extensively studied in the terrestrial inner magnetosphere (e.g. Burtis & Helliwell, 1969, 1976; Tsurutani & Smith, 1974) and also identified in the magnetospheres of Jupiter (Coroniti et al., 1980; Scarf et al., 1981; Menietti, Horne, et al., 2008), Saturn (Hospodarsky et al., 2008; Menietti, Santolik, et al., 2008), and Mars (Harada et al., 2016). In the terrestrial magnetosphere, chorus emissions are known to be excited near the magnetic equator, where resonant electrons tend to be abundant because the magnetic field strength is minimal and therefore the resonant velocity is small. Chorus emissions have been implicated in diffuse auroras and the outer radiation belt through electron acceleration (Horne et al., 2005; Thorne et al., 2013). A characteristic feature of chorus emissions is rising (or falling) tone elements, in which the frequency rises (or falls) in a short period less than 1 second. The generation of the rising tone can be explained by the nonlinear growth theory, which takes into account the second-order terms of cyclotron resonance (Omura et al., 2008; Omura, 2021). Simulations (Omura et al., 2008; Katoh & Omura, 2011) reproduce the rising tone, and also the time evolution of the rising frequency and the growing amplitude in simulations and observations show a good agreement with the theory (Cully et al., 2011; Kurita et al., 2012).

Another typical feature of chorus emissions is a two-band structure in the spectrum with an intensity gap around 0.5 f_{ce}, making a separation into two frequency bands, the lower band and the upper band (Burtis & Helliwell, 1969, 1976; Tsurutani & Smith, 1974). Teng et al. (2019) have statistically demonstrated the common presence of two-band structure in the terrestrial whistler-mode waves, showing the ratio of two-band to no-gap waves is 3:1 in the observations of Van Allen probes. Similarly, Gao et al. (2019) found a 2:1 ratio of multi-band and no-gap waves in the Time History of Events and Macroscale Interactions during Substorms (THEMIS) magnetic field waveform data from a statistical analysis using different criteria. Despite decades of research, the formation mechanisms of the two-band structure remain a long-standing question. One of the leading hypotheses is that Landau damping creates an intensity gap at 0.5 f_{ce} (Tsurutani & Smith, 1974; Omura et al., 2009). They have proposed that a rising tone is first excited as a continuous element extending over both bands and propagates parallel to the field line. During the propagation, the waves gradually becomes oblique and exhibit an electrostatic component due to the curvature of the field line at the off-equator, which causes the Landau resonance. In some circumstances (i.e. electrons bouncing between magnetic mirrors), 0.5 f_{ce} waves can be efficiently Landau-damped by co-streaming electrons in cyclotron resonances with counter-streaming waves, because the cyclotron resonance velocity equals in the magnitude but opposite to the wave phase velocity (Tsurutani & Smith, 1974). The propagation of waves widens the gap as an off-equatorial f_{ce} increases from the equatorial f_{ce} with the increasing magnetic field strength. Gao et al. (2016) proposed another mechanism called the lower band cascade mechanism, in which upper band waves are excited as a harmonic structure through the coupling of a lower band electromagnetic wave with an electrostatic density mode wave of approximately equal frequency. In another study, Fu et al. (2014) argued from PIC simulation results that the lower and upper bands can be generated by two anisotropic electron components with different temperatures, and that a gap is formed between them as a natural consequence. Each of these theories alone cannot fully explain observed results as follows. Habagishi et al. (2014) supported the Landau damping scenario by showing a clear correspondence of higher and lower frequency edges of the gap with the local 0.5 f_{ce} and the equatorial 0.5 f_{ce}. On the other hand, smaller occurrence rates of no-gap events near the magnetic equator are contrary to the consequences from the Landau scenario (Teng et al., 2019; Gao et al., 2019). Gao et al. (2019) have suggested that power gaps could be a result of a combination of several different mechanisms, based on two types of banded chorus different in the intensity and electrostatic nature of upper band waves.

Unlike the Earth, the Moon is an airless body with no global intrinsic magnetic field. As the Moon orbits around the Earth, it passes through the solar wind, terrestrial magnetosheath, and terrestrial magnetotail. These regions are characterized by very different plasma parameters, so the external plasma surrounding the Moon is greatly variable (e.g. Harada & Halekas, 2016). In addition, the lunar surface is known to be electrostatically charged in response to the input and output of charges from and to the ambient plasma (Whipple, 1981). The lunar surface charging is determined by the balance between the charged particle flux absorbed by the lunar surface and that emitted from the surface. On the sunlit surface, the dominant current is a downward current toward the lunar surface provided by photoelectrons emission, which results in a positive charge and positive potential on the day side. On the night side of the Moon, the ambient electron current prevails because of a higher thermal speed of electrons than ions, and thus the accumulated negative charge results in a negative electrostatic potential.

Recent observations revealed the presence of whistler-mode waves excited near the Moon (Halekas, Poppe, Farrell, et al., 2012; Harada et al., 2014, 2015). Moon-related whistler-mode waves are excited by upward traveling electrons along field lines connected to the Moon. The free energy source for the wave excitation is provided by an effective temperature anisotropy in upward electrons resulting from the anisotropic reflection; incident electrons with larger pitch angles are reflected by lunar crustal magnetic fields while smaller pitch angle electrons are absorbed at the lunar surface. Harada et al. (2014) found that the intensity of whistler-mode waves is generally weakened on field lines connected to strong magnetic anomalies, which could be attributable to the reduction of the effective temperature anisotropy due to stronger magnetic magnetic reflection leading to more isotropic distributions of upward traveling electrons. Furthermore, Sawaguchi et al. (2021) reported that lunar whistler-mode waves can form chorus-like rising tone elements consistent with the nonlinear growth theory of Omura et al. (2008) in the relationship between frequency sweep rates and the amplitudes. The presence of rising tone elements at the Moon suggests that a common physical process can operate for whistler-mode waves both at the Moon and in the terrestrial inner magnetosphere, and that the lunar environment provides a useful test case for chorus research. However, another typical feature of chorus emissions, the two-band structure, has not been investigated and it remains unclear whether it exists around the Moon or not.

In this study, we conduct a statistical study of spectral properties of whistler-mode waves in the vicinity of the Moon by utilizing Acceleration, Reconnection, Turbulence, and Electrodynamics of the Moon's Interaction with the Sun (ARTEMIS) observations. Following the methodology of Teng et al. (2019) for the terrestrial inner magnetosphere, we classify spectral shapes of the Moon-related whistler-mode waves into four categories, including the two-band structure, and statistically investigate their occurrence rates. In addition, we also investigate variations of the spectral properties in different plasma environments of the Moon. These investigations could provide further insights into the universality of the proposed generation mechanisms of the two-band chorus emissions and into the temporally and spatially variable plasma environment around the Moon.

2 Data and methodology

We analyze data obtained by the ARTEMIS mission (Angelopoulos, 2011) from July 2011 to June 2020. We utilize onboard FFT spectra of wave magnetic field from Search Coil Magnetometer (SCM; Roux et al., 2008) and background magnetic field vector data from Fluxgate Magnetometer (Auster et al., 2008).

We process the onboard FFT data in the following manner. We first exclude intense broadband noise, which is likely to be caused by artificial contamination such as spike noises, from statistics by rejecting a spectrum if the power given by integrating the power spectral density over frequencies above $1f_{ce}$ exceeds 10^{-5} nT^2. Then we perform automatic identification of whistler-mode waves and classification of them according to their spectral shapes by adapting the methodology of Teng et al. (2019). For a given spectrum as a function of the wave frequency f, we identify a whistler-mode wave event if the maximum power spectral density in a frequency range of $0.1 < f/f_{ce} < 0.8$ is larger than a threshold value of $p_{th} = 10^{-6}$ nT^2/Hz. Note that the threshold value is set two orders of magnitude higher than Teng et al. (2019) to take into account the higher noise floor of the SCM onboard spectra in the corresponding frequency range than that of burst mode wave data by Van Allen probes used in Teng et al. (2019). Also, the frequency range is restricted to above 10 Hz because the data below 10 Hz contain a considerable amount of noises. In addition, if the aforementioned maximum power does not form a peak with a positive spectral slope in the frequency range of $0.1 < f/f_{ce} < 0.8$ and $f > 10$ Hz, the data point is treated as "no wave" to avoid misdetection of a part of other lower frequency waves.

Next, the identified whistler-mode wave events are classified into four categories of spectral shapes: lower band only, upper band only, no-gap, and banded waves. Figure 1 shows examples of the spectrum of the four types of events. The gap frequency f_{gapmin} is defined as the frequency at which the power of the wave takes the minimum value p_{gapmin} within a frequency range of $0.45 < f/f_{ce} < 0.55$. Then the power of lower band and upper band, p_L and p_U, are defined as the maximum values within $0.1f_{ce} < f < f_{gapmin}$ and $f_{gapmin} < f < 0.8f_{ce}$, respectively. If $p_L > p_{th}$ and $p_U < p_{th}$, then the waves are identified as lower band only waves. The case of $p_L < p_{th}$ and $p_U > p_{th}$ is defined as upper band only waves. In cases that both p_L and p_U are higher than p_{th}, those events with p_L and p_U both of which are higher than $10^{1.5}p_{gapmin}$ are defined as banded waves, and the rest are considered as no-gap waves. We also tested the algorithm using THEMIS data obtained in the terrestrial inner magnetosphere and validated that the algorithm is capable of discriminating between the banded and no-gap waves with onboard FFT spectra of THEMIS-ARTEMIS/SCM (see Supporting Information for details).

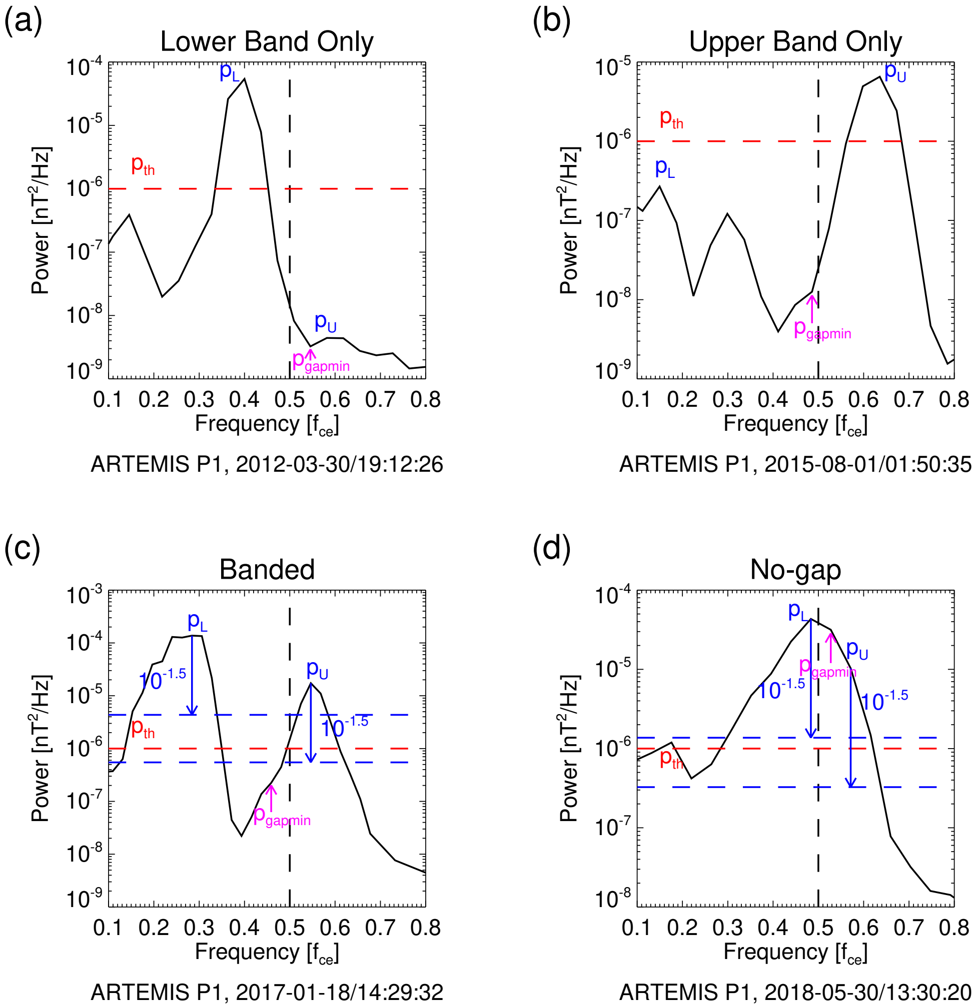

Figure 1. Examples of spectra of events observed by ARTEMIS SCM. Each panel shows different classifications of four types of spectral shapes: (a) Lower band only, (b) Upper band only, (c) Banded, and (d) No-gap. In all panels, the vertical black dashed line indicates 0.5 f_{ce} and the horizontal red dashed-and-dotted line represents the threshold power spectral density, $p_{th} = 10^{-6}$ nT^2/Hz. In panels (c) and (d), $10^{-1.5}p_L$ and $10^{-1.5}p_U$ are shown by the horizontal blue dashed lines.

3 Results

Plasma properties in the near-Moon space vary significantly in time and space. Consequently the wave excitation condition also changes, and it is necessary to separate the statistics by the plasma environment. First, we organize the data into coordinates relevant to the field line connection to the Moon under a straight field line assumption (Figure 2), because the connection of the observation point to the Moon by magnetic field lines is suggested to be a key controlling factor for the excitation of whistler-mode waves (Halekas, Poppe, Farrell, et al., 2012; Harada et al., 2014, 2015). As illustrated in Figure 2b, for a given spacecraft position and a measured magnetic field vector, we extrapolate a straight field line from the spacecraft. We calculate the minimum distance between the straight field line and the center of the Moon (hereafter termed "B distance"), and the distance from the spacecraft to the point at which the field line is closest to the center of the Moon ("SC distance"). If we display this coordinate system with the SC and B distances on the X and Y axes, respectively, a simple condition of $Y < 1\mathrm{R_L}$ indicates the magnetic field line connection to the Moon under the straight field line assumption. In practice, the assumption may not be valid due to the field line curvature, and the boundary of connected and unconnected conditions may not be perfectly distinct at $Y = 1\mathrm{R_L}$. Figure 2a shows the SC distance–B distance distribution of the occurrence rate (defined as the fraction of observed spectra showing the wave events in each bin) of all events for all observations, regardless of the event types. The occurrence rate increases over an order of magnitude for $Y < 1\mathrm{R_L}$, indicating that the field-line connection controls the excitation of the whistler-mode waves. As the SC distance increases, the boundary of high- and low-occurrence rate regions becomes increasingly blurred, as expected from field lines with finite curvature. Nevertheless, the enhanced occurrence rate at $Y < 1\mathrm{R_L}$ is clearly visible even at $X > 10\mathrm{R_L}$ around the apoapsis of ARTEMIS, and hereafter we classify events with $Y < 1\mathrm{R_L}$ as Moon-related wave events.

Next, the external plasma environment is separated, to first order, according to the position of the Moon. For simplicity and full use of available FFT data, we use the GSE longitude, θ_{GSE}, of the Moon (full moon as seen from the Earth corresponding to $\theta_{GSE} = 0°$) and classify the plasma regime into three categories, the solar wind (SW; $53° < \theta_{GSE} < 293°$), magnetosheath (MS; $27° < \theta_{GSE} < 53°$ and $293° < \theta_{GSE} < 327°$), and magnetotail (MT; $\theta_{GSE} < 27°$ and $327° < \theta_{GSE}$), based on the average ion properties derived from long-term ARTEMIS data by Poppe et al. (2018). It should be noted that

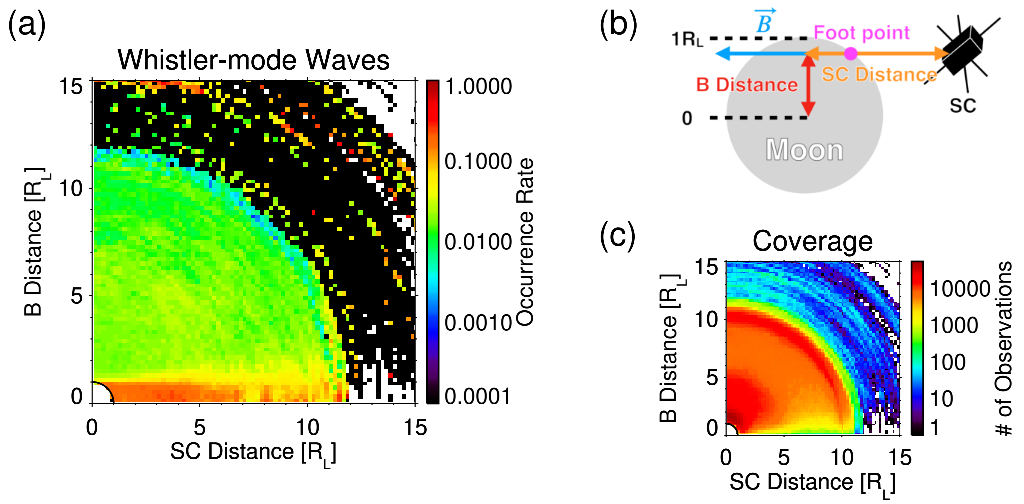

Figure 2. (a) Occurrence rate distribution of all types of events in all regions. The Y-axis represents the minimum distance in lunar radii between the magnetic field line and the center of the Moon, and the X-axis represents the distance in lunar radii from the spacecraft to the point at which the field line is closest to the center of the Moon. (b) Schematic illustration of the coordinate system used in panel (a). (c) Number of all observations shown in the same format as panel (a).

this classification is only an approximation and each category is likely to include some observations in adjacent plasma regimes.

Figures 3-5 show the occurrence rate distributions in the same format as Figure 2a, except that they are classified by the external plasma environment and wave spectral shapes. Although the upper band only events in the solar wind (Figure 3b) and magnetosheath (Figure 4b) as well as the banded events in all regions (Figures 3c, 4c, and 5c) are too rare to discern any meaningful trend, the occurrence rates of the other classifications clearly increase for $Y < 1\mathrm{R_L}$. The higher occurrence rates within $Y < 1\mathrm{R_L}$ confirm once again that magnetic field line connection to the Moon is an important factor in the excitation of whistler-mode waves, and in the following analysis we will focus on these Moon-related wave events at $Y < 1\mathrm{R_L}$. We note that a relative increase is observed in the occurrence rate of lower band only events at $Y > 1\mathrm{R_L}$ in the magnetosheath (Figure 4a), possibly due to the detection of lion roars originally present in the background magnetosheath plasma (Smith & Tsurutani, 1976). As shown in Figure 6, the number

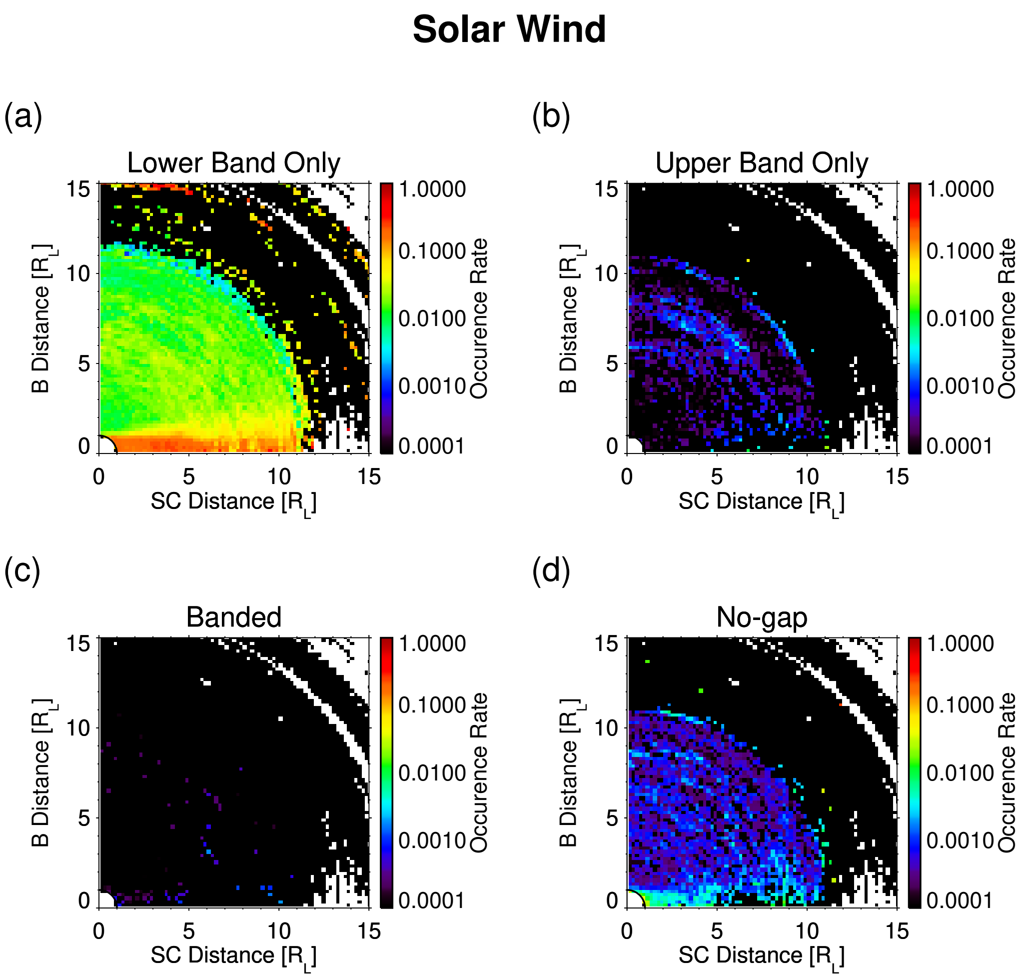

Figure 3. Occurrence rate distributions of four types of whistler-mode wave events in the solar wind. Each panel is in the same format as Figure 2

of observation points, which represent the denominator of the occurrence rate, is sufficiently large within $X <\sim 11\mathrm{R_L}$.

Solar radiation is also an important driver in the lunar plasma environment. For example, photoelectrons are emitted from the dayside lunar surface, leading to positive surface charging on the day side of the Moon. On the night side, in addition to negative charging of the lunar surface driven by a predominant ambient electron current, the lunar wake is formed downstream of the solar wind. Hence, we divide the Moon-related events into dayside and nightside events based on the solar zenith angle at the foot point of the magnetic field line. Events with solar zenith angles $< 90°$ ($> 90°$) are classified

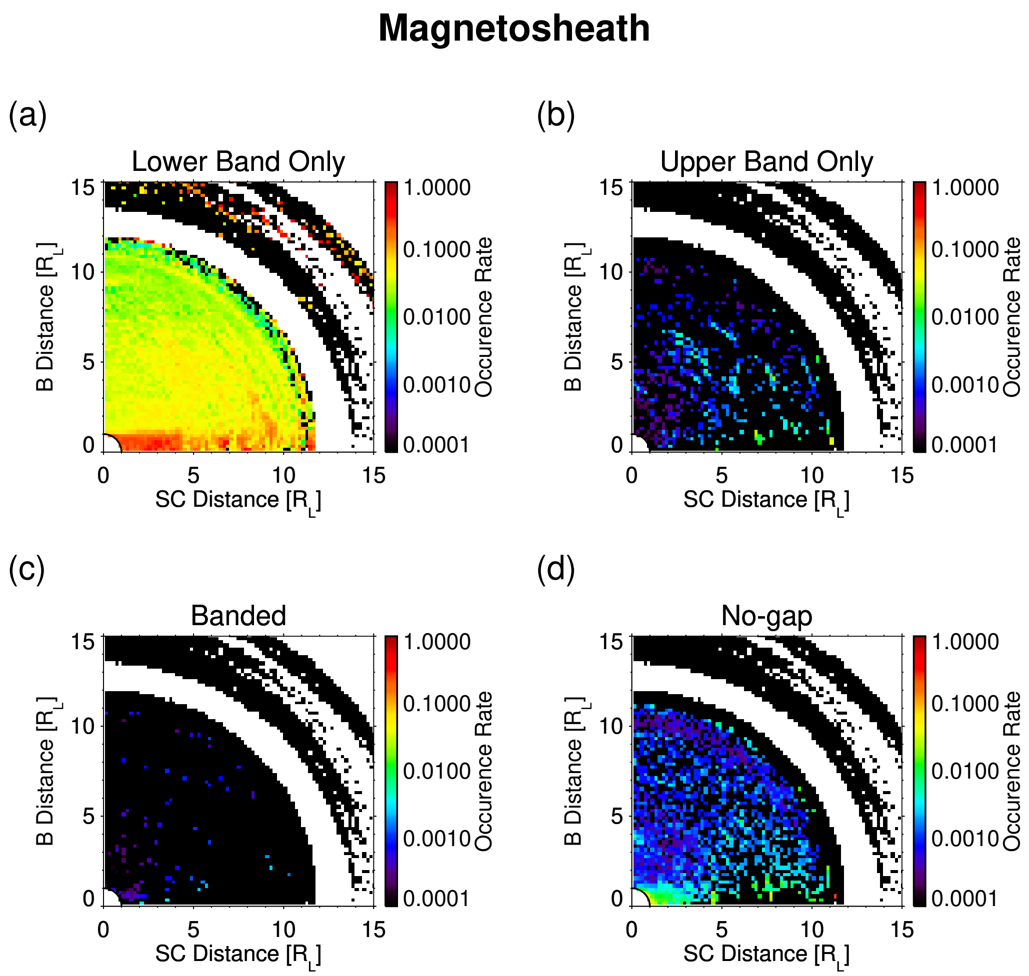

Figure 4. Occurrence rate distributions of four types of whistler-mode wave events in the magnetosheath. Each panel is in the same format as Figure 2

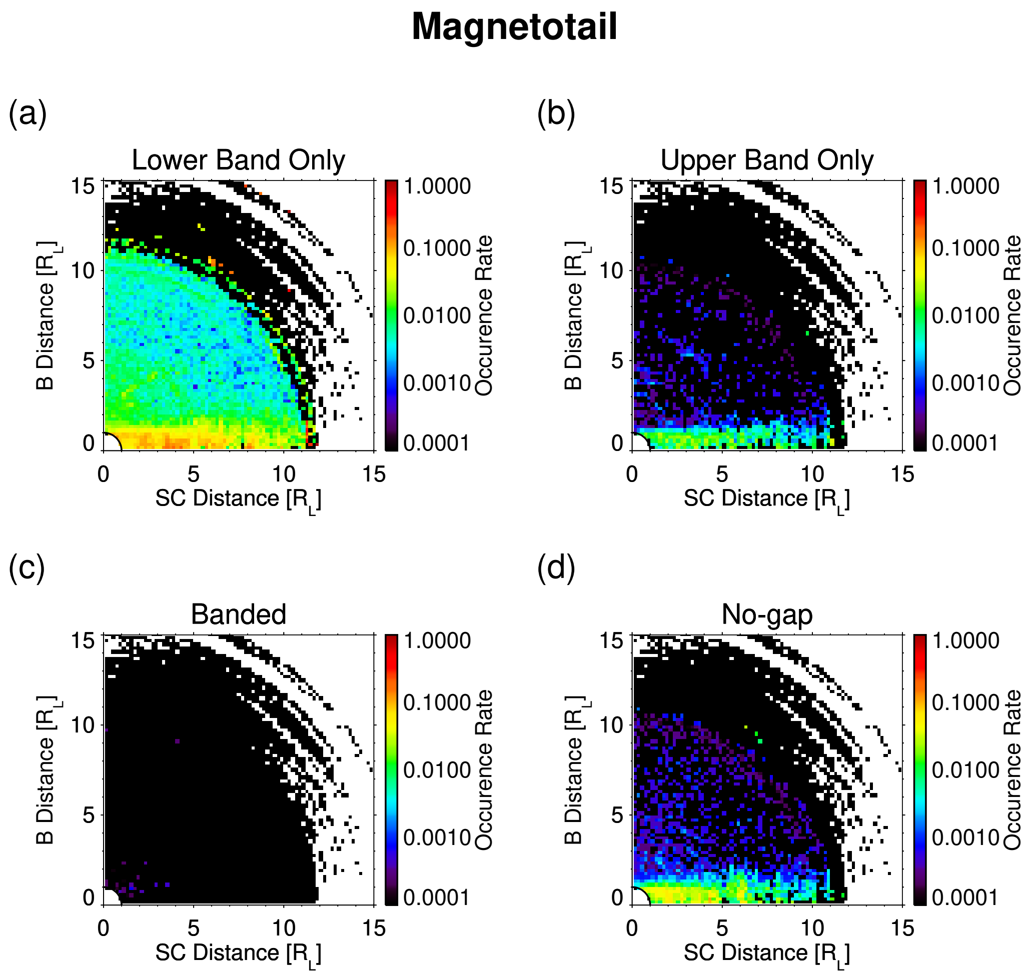

Figure 5. Occurrence rate distributions of four types of whistler-mode wave events in the magnetotail. Each panel is in the same format as Figure 2

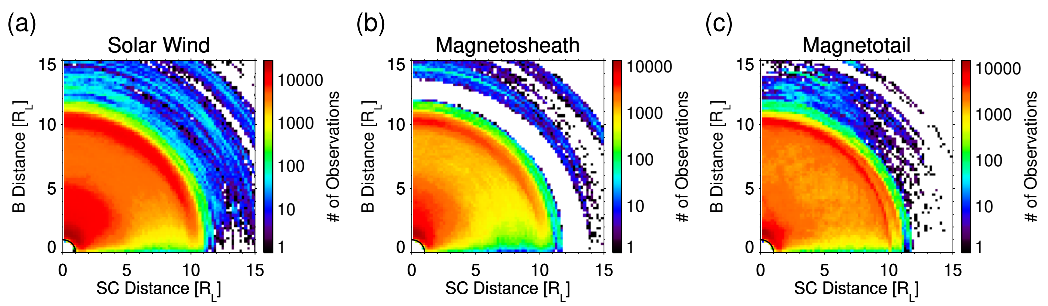

Figure 6. Observation point distributions in the solar wind, magnetosheath, and magnetotail. Each panel is in the same format as Figure 2 except that the color indicates the total number of observations in each bin.

Table 1. Number (occurrence rate) of whistler-mode wave events classified by day/night at foot point of the magnetic field line and the location of the Moon.

Day/Night	Region	Data points	Wave events
Day	SW	360,289	81,005 (22.5%)
	MS	86,961	28,068 (32.3%)
	MT	165,105	21,839 (13.2%)
Night	SW	248,591	14,658 (5.90%)
	MS	77,833	6,362 (8.12%)
	MT	110,186	8,462 (7.68%)

as dayside (nightside) events. Tables 1 and 2 show the results for the day-night conditions subdivided by the external plasma environment.

First, we point out that very few banded events are identified while the no-gap events rank the second most common type for any circumstances shown in the rows of Table 2. The banded to no-gap ratio of <0.05 is markedly different from $\sim$2–3 in the terrestrial inner magnetosphere (Teng et al., 2019; Gao et al., 2019). We note that this difference is unlikely to arise from the differences in the algorithm or data as demonstrated in Supporting Information. Second, the ratio of upper band only to no-gap events is larger in the magnetotail than in the other two regions regardless of day or night (Table 2), indicating that upper band only events are rarely observed in the solar wind and in the magnetosheath. Third, in comparison between the day and night conditions, the occurrence rates are clearly higher on the day side (Table 1).

To investigate the influence of the lunar magnetic anomalies on Moon-related waves, we map the occurrence rates in the selenographic coordinates based on the foot point longitude and latitude, separately for the dayside and nightside events. Figures 7-9 show the occurrence rates in the selenographic coordinates in the solar wind, magnetosheath, and magnetotail. The contours in solid black and magenta lines indicates a crustal field strength of 2 nT at a 30 km altitude evaluated by the lunar magnetic anomaly model of Tsunakawa et al. (2015). Note that the observation points in these distributions are heavily biased in longitude owing to the geometrical constraints of the lunar orbit (panels a and f in Figures 7-9). Also note that, as only few events are identified, no mean-

Table 2. Number (ratio) of four types of events classified by day/night at foot point of the magnetic field line and the location of the Moon.

Day/Night	Region	Lower	Upper	Banded	No-gap
Day	SW	78,656 (97.1%)	44 (0.05%)	43 (0.05%)	2,262 (2.79%)
	MS	26,975 (96.1%)	33 (0.12%)	19 (0.07%)	1,041 (3.71%)
	MT	11,659 (53.4%)	2,842 (13.0%)	13 (0.06%)	7,325 (33.5%)
Night	SW	14,453 (98.6%)	18 (0.12%)	7 (0.05%)	180 (1.23%)
	MS	6,180 (97.1%)	38 (0.60%)	6 (0.09%)	138 (2.17%)
	MT	7,546 (89.2%)	295 (3.49%)	2 (0.02%)	619 (7.32%)

ingful trend can be discerned for the upper band only and banded (Figures 7c, 7d, 7h and 7i) and no-gap (Figure 7j) in the solar wind, the upper band only and banded (Figures 8c, 8d, 8h and 8i) in the magnetosheath, and the banded (Figures 9d and 9i) in the magnetotail. In the other cases, the occurrence rates generally decrease near the magnetic anomalies as suggested by Harada et al. (2014). However, we also find two features that contradict this trend: (i) there exists a high occurrence area around Reiner Gamma ($-20°$ to $20°$ latitudes and $-90°$ to $-60°$ longitudes) regardless of the lunar circumstances and the spectral shapes; and (ii) for the lower band only events on the night side in the solar wind and magnetosheath (Figures 7g and 8g), high occurrence rates are seen in several longitude and latitude bands with no apparent association with magnetic anomalies.

4 Discussion

4.1 Two-band structure formation

The statistical results show that no-gap whistler-mode waves are much more common than banded waves with detectable gaps around the Moon, suggesting that the $0.5f_{ce}$ gap generation mechanisms are not as effective around the Moon as they are in the terrestrial inner magnetosphere. Here we discuss the applicability of the gap generation scenarios to the Moon-related whistler-mode waves.

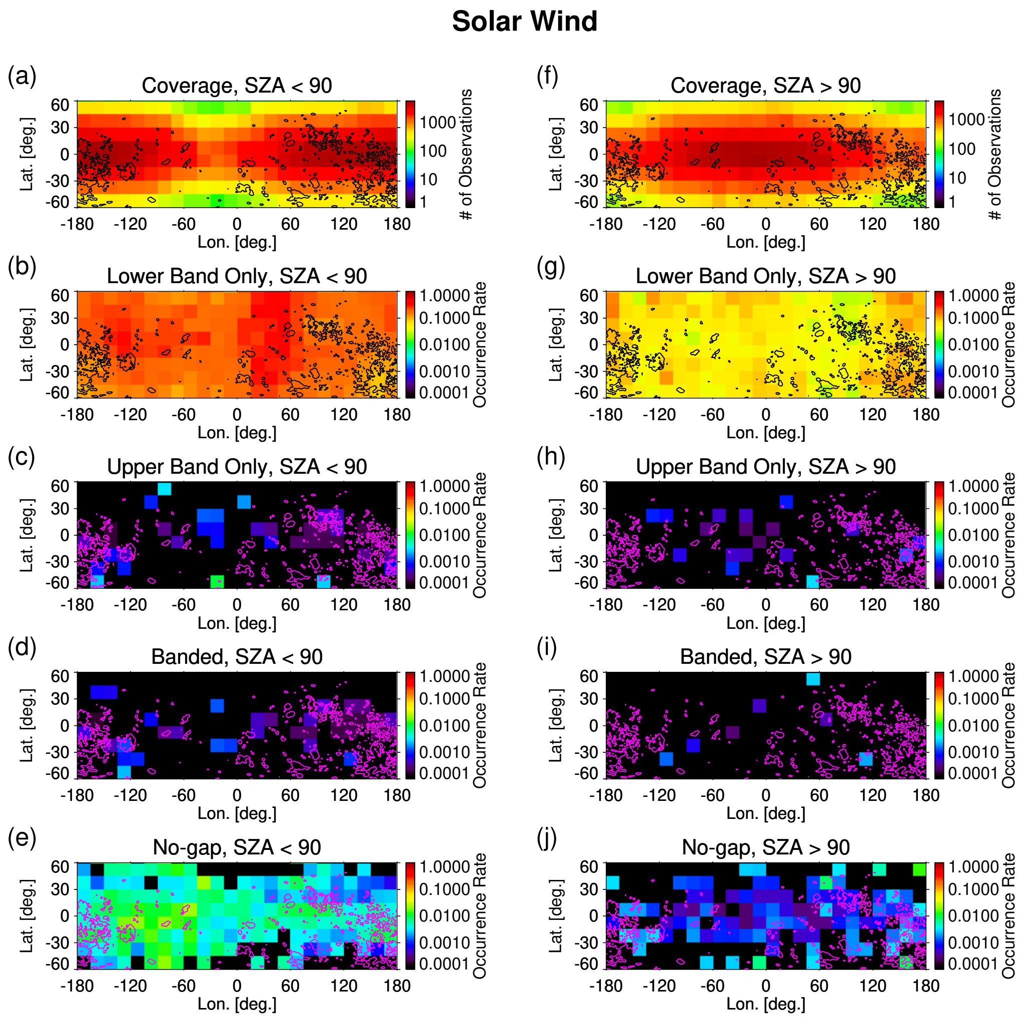

Figure 7. (a) Number of observations when the background magnetic field line is connected to the day side of the Moon in the solar wind and (b-e) occurrence rates of four types of whistler-mode wave events as a function of selenographic locations of the field line foot point. Panel (f) and Panels (g-j) are the same data as panel (a) and panels (b-e) except that the background magnetic field line is connected to the night side of the Moon. The contours in solid black and magenta lines indicates a crustal field strength of 2 nT at a 30 km altitude evaluated by the lunar magnetic anomaly model of Tsunakawa et al. (2015).

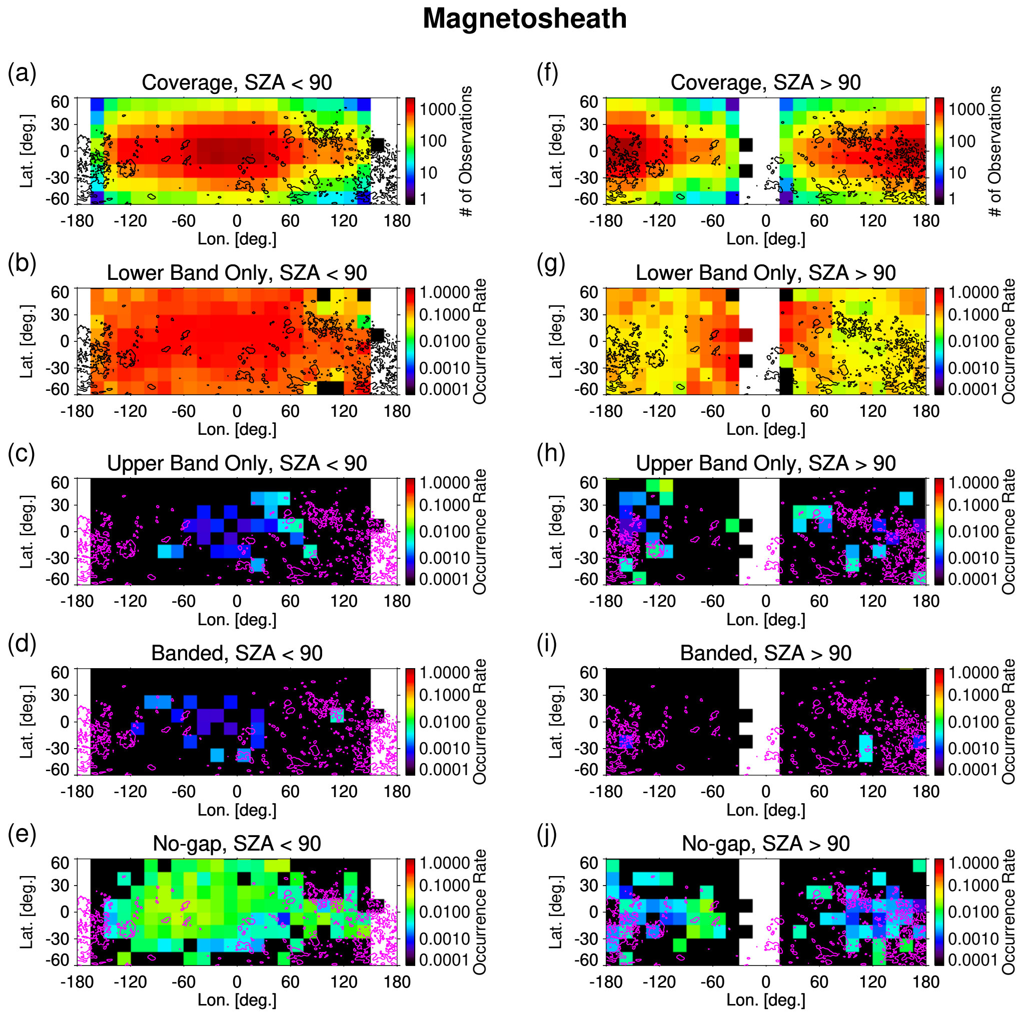

Figure 8. Selenographic distributions of observation points and event occurrence rates in the magnetosheath in the same format as Figure 7.

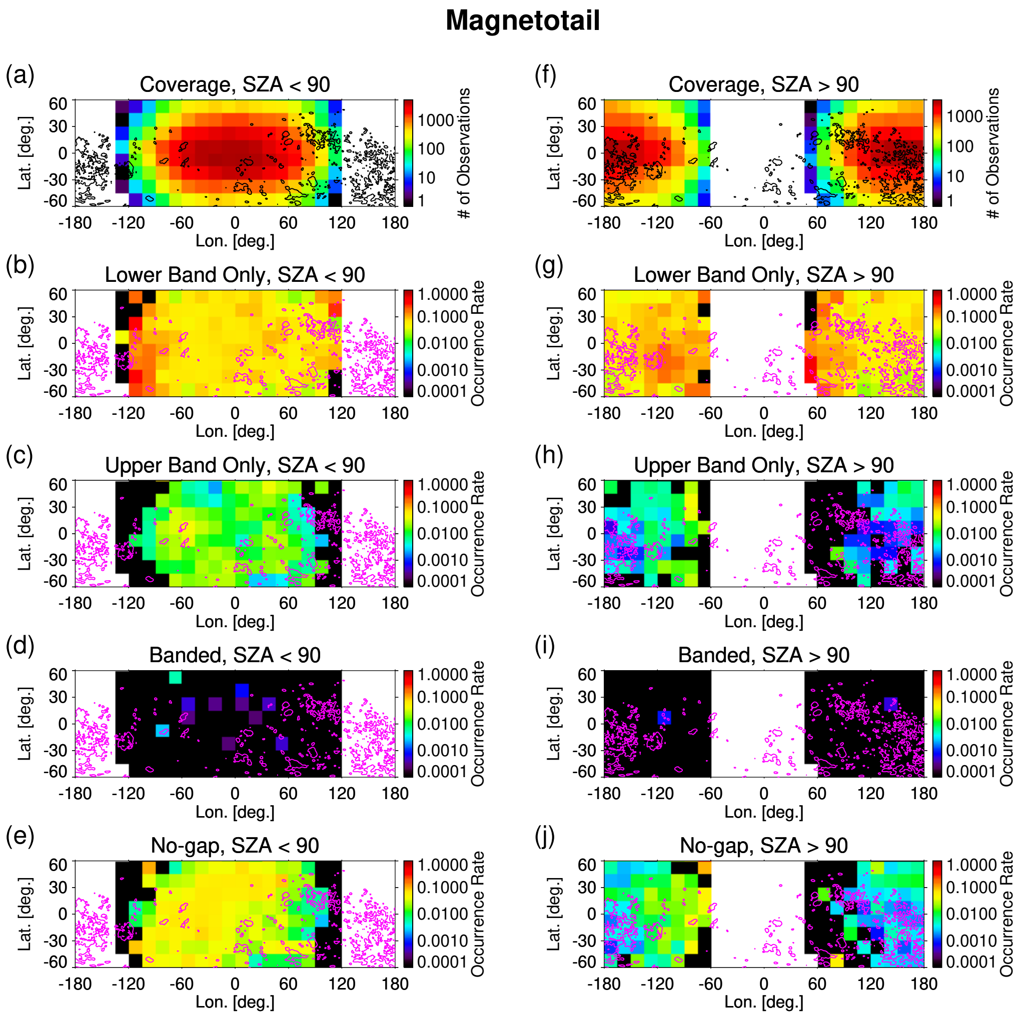

Figure 9. Selenographic distributions of observation points and event occurrence rates in the magnetotail in the same format as Figure 7.

First, in the Landau damping gap formation scenario for terrestrial chorus emissions (Tsurutani & Smith, 1974; Omura et al., 2009), a broad band wave is excited in the equatorial source region and subsequently propagates to higher latitudes, widening the gap at the local $0.5f_{ce}$ due to the increase of the field strength. In contrast, at least for typical conditions in the solar wind and magnetotail, one of the possible explanations for the absence of banded events could be provided by the $0.5f_{ce}$ variation being too small to generate a detectable gap. To a first-order approximation, the field-aligned gradient of the magnetic field strength around the Moon is expected to be negligible. For typical conditions in the solar wind, incompressible Alfvénic disturbances prevail, and the field strength fluctuations are small (Khabibrakhmanov & Summers, 1997). In the magnetotail at the lunar orbit 60 Earth radii downstream of the Earth, the magnetic field lines are highly stretched along the Sun-Earth line, and the magnetic field strength may be more or less uniform along the field lines except for dynamically formed structures (e.g., plasmoids) during geomagnetically disturbed conditions. On the other hand, since compressible disturbances dominate in the magnetosheath, as typified by the mirror mode structure, the gradient of the magnetic field strength should be large (Tsurutani et al., 1982), and this argument cannot explain why the banded waves were not observed in the magnetosheath. In order to assess the effectiveness of the gap formation by Landau damping, the magnetic field gradient around the Moon should be quantitatively evaluated from observations in each plasma regime, but this is beyond the scope of this paper.

Another explanation for the absence of a Landau damped gap is that the waves are generally observed inside the source region because the whistler-mode waves travel toward the lunar surface in cyclotron resonance with upward traveling electrons. This situation is essentially different from the terrestrial chorus emissions, for which the waves are commonly observed after the propagation away from the source region localized near the magnetic equator. Therefore, the formation of a deep gap by Landau damping during propagation is unlikely to occur for the Moon-related whistler-mode waves, because even if Landau damping did occur, the damped area in the spectrum would be immediately filled by further wave excitation.

A simple extrapolation of the lower band cascade scenario for terrestrial chorus emissions to the Moon-related whistler-mode waves cannot explain the absence of banded events. In the lower band cascade scenario in the Earth's magnetosphere, the lower band wave amplitude exceeding $\sim$100 pT is a necessary condition for the formation of a two-band structure by subsequent excitation of the upper band waves (Gao et al., 2016). Figure 3 in Sawaguchi et al. (2021) shows a lower band only event with rising tone elements observed around the Moon, whose magnetic field amplitude exceeds 100 pT, seemingly satisfying the upper band excitation threshold. In our statistical results, banded waves are almost absent, despite the intensity of observed waves as large as those in the Earth magnetosphere. Note, however, that in the lower band cascade scenario, the upper band may be electrostatic and the two-band structure may be seen only in the electric field (Gao et al., 2019). Since our analysis did not examine the electric field, we cannot distinguish lower band only waves from this type of banded waves caused by the cascade scenario.

We next discuss the scenario proposed in Fu et al. (2014), in which the two electron components excite the lower and upper bands separately. There seems to be generally no mechanism to separate electrons with temperature anisotropy into two components at the Moon, and we conclude that this two component scenario is not applicable to the Moon-related whistler-mode waves. Considering that the electron anisotropy at the Moon originates from a loss cone due to electron absorption at the lunar surface, it is implausible that the driving anisotropic electrons consist of two separated components at high and low energies, and such peculiar electron distributions have not been reported so far to the best of our knowledge.

4.2 An example of banded events

For more detailed discussion on the gap formation mechanisms, we next look at a specific example shown in Figure 10 among the rare banded events. This event was observed in the solar wind (Figures 10a, 10e, and 10i), P1 and P2 happened to be located on nearby magnetic field lines (Figure 10a), and P1 and P2 observed the loss cone of the upward (parallel) electrons formed by lunar surface absorption (Figures 10f and 10j) and the electromagnetic waves below and above 0.5 f_{ce} (Figures 10g and 10k). One of the most remarkable features is the temporary disappearance of the lower band wave and the loss cone structure of the upward-traveling electrons observed by P1 at around 21:13 UT (indicated by the arrows in Figures 10j and 10k), indicating that the magnetic field line was disconnected from the Moon at this timing. Simultaneously, the change in the direction of the background magnetic field was observed (Figure 10h). The magenta arrows in Figure 10b indicate the three data points that were classified as banded events. While the lower band was nearly continuously observed, the upper band signatures were only intermittently detected. The wave intensity of the lower band decreased from 21:44:40 to 21:45:00 UT, and at the same time the size of the loss cone of 100 to 500 eV electrons became narrower (Figures 10b and 10d). Based on calculation of the resonance velocity, these electrons shown in Figure 10d corresponds well to the resonant electrons for the lower band. In Figure 10b, upper band waves were also observed just before the banded events indicated by the arrows, although their intensity was lower than the event selection threshold. These upper band waves have no apparent association with the pitch angle distributions of 10-20 eV electrons (Figure 10c), which are expected to be in cyclotron resonance with the waves at $\sim$0.5–0.6f_{ce}. Looking again at the dynamic spectra in Figures 10g and 10k, we can see intermittent observations of the upper band while the lower band continues for a few to tens of minutes. The frequency of the "upper band" wave component with small intensity varied greatly in the time series, and in fact, its frequency dropped below 0.5f_{ce} for some instances. It is also noteworthy that the upper band-like component was observed even around 21:13 UT, when the magnetic field line was temporarily disconnected as mentioned above.

We now discuss possible generation mechanisms of the two-band structure in this event. The Landau damping scenario, in which an originally continuous rising tone component extending over both bands is split into two by Landau damping, is inadequate to explain the uncorrelated generation of the lower band and upper band as seen in this event. In the lower band cascade scenario, the upper band should be excited as a harmonic about twice as high as the lower band, but this is not the case for this event because the frequencies of the lower band and upper band are obviously not harmonically related. The scenario with separate wave excitation by the two anisotropic electron components is hard to be reconciled with the observed electron distributions. Considering these facts, we speculate that this event may be a coincident detection of lower band whistler-mode waves excited at the field line foot point and higher frequency whistler-mode waves propagating from a different wave source, and the two waves are coincidentally present at the observed location. In the P1 data, the connection of the magnetic field lines to the Moon is lost around 21:49 UT, and concurrently the intense component of the lower band is no longer observed, while the weak wave component at a relatively high frequency at $\sim$150 Hz (0.4f_{ce}) is continuously observed until about four minutes later (Figures 10j and 10k). Moreover, no upper band waves were observed in P2 before 21:38 UT (Figure 10g), when the field line connection started as is evident from the appearance of the

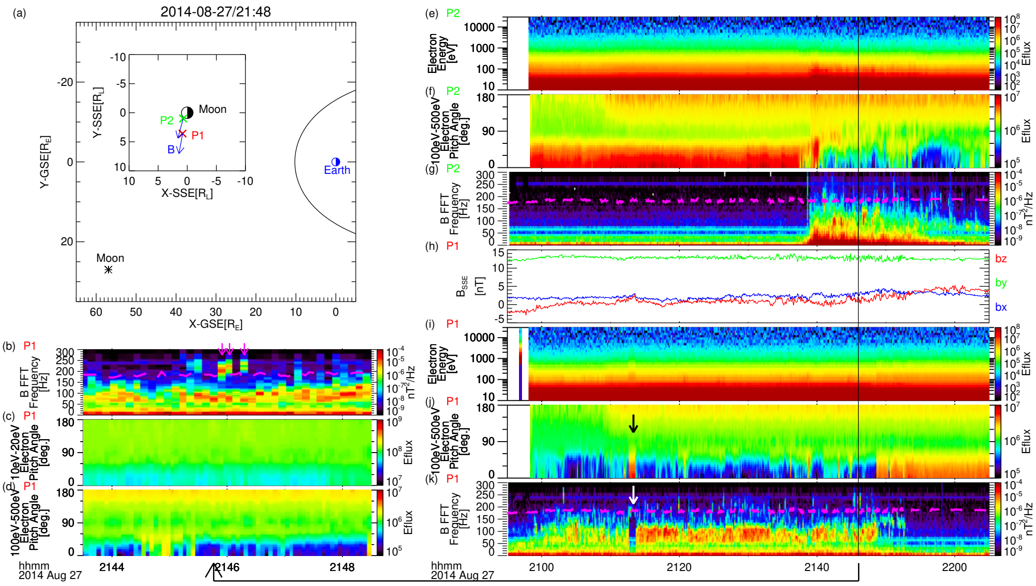

Figure 10. ARTEMIS observations of banded wave events on August 27, 2014. (a) The position of the Moon in the geocentric solar ecliptic (GSE) coordinate system, where the blue circle, the black asterisk, and the black line represent the Earth, the Moon, and a typical magnetopause location (Shue et al., 1997), respectively. The inset shows the positions of the probes in the selenocentric solar ecliptic (SSE) coordinate system, where the black circle, and red and green X-marks, and blue arrows represent the Moon, P1 and P2, and magnetic field direction, respectively. Time series data from ARTEMIS P1 at 21:43:30–21:48:30 UT of (b) magnetic wave spectra and pitch angle spectra of (c) 10–20 eV and (d) 100–500 eV electrons in units of differential energy flux (labeled "Eflux" for short, eV/cm2/sr/s/eV). Time series data from ARTEMIS P1 and P2 at 20:55–22:05 UT of (e, i) energy spectra of electrons in units of differential energy flux, (f, j) pitch angle spectra of 100 –500 eV electrons in units of differential energy flux, (g, k) magnetic wave spectra, (g) magnetic fields in the SSE coordinate system. The data shown in panels (h–k) and panels (e–g) are obtained by P1 and P2, respectively. The dashed magenta lines in panels (g) and (k) represent half the electron cyclotron frequency. Banded events are denoted by the magenta arrows in panel (b).

electron loss cone (Figure 10f), indicating no clear wave activity in the pristine solar wind. These results suggest that whistler-mode waves generated on another magnetic field line connected to the lunar surface at a different foot point may have propagated across the magnetic field line with an oblique propagation angle. Unfortunately, no burst-mode waveform magnetic field data are available for this time, so the propagation angle cannot be examined.

4.3 Dependences on the external and local plasma environments

In Section 3, notable differences are identified in the occurrence rates of whistler-mode wave events depending on the magnetic connection to the Moon, the position of the Moon, and the day/night condition and the selenographic location of the field-line foot point. First, it is directly demonstrated from the occurrence rates that the magnetic field line connection to the Moon is a dominant controlling factor in whistler-mode wave excitation, also consistent with case studies and average wave power statistics in the previous studies (Halekas, Poppe, Farrell, et al., 2012; Harada et al., 2014).

Next, on field lines connected to the night side of the Moon, the wave occurrence rate is smaller than the day side regardless of the frequency band and the position of the Moon. Also, the occurrence rate of upper band waves is suppressed in the solar wind and magnetosheath compared to that in the magnetotail. We explain these suppressions by small anisotropy resulting from enhanced reflection of electrons above the lunar surface. The nightside lunar surface is negatively charged, and the negative electrostatic potential reflects incident electrons with low parallel energies. As the reflected electrons fill the otherwise empty loss cone, the electrostatic reflection reduces the effective temperature anisotropy, possibly leading to the suppressed wave occurrence on field lines connected to the nightside lunar surface. The small anisotropy at low energies resulting from the electrostatic reflection would lead to suppression of high frequency whistler-mode waves. This can explain the reduced relative occurrence of upper band events on the night side in the magnetotail with respect to that on the day side in the magnetotail. The low occurrence of upper band events on the day side in the solar wind and magnetosheath compared to that in the magnetotail could be explained in a similar manner; for magnetic reflection (or electrostatic reflection if a downward electric field exists) from the day side of the Moon in a fast moving plasma such as the solar wind and magnetosheath flow, the reflected electrons are effectively accelerated in the plasma reference frame because of the moving obstacle effect (Halekas, Poppe, Farrell, et al., 2012; Halekas, Poppe, Delory, et al., 2012). This effect shifts the reflected component toward higher parallel velocities in the plasma frame, effectively reducing the electron anisotropy at lower energies and suppressing whistler-mode wave excitation at higher frequencies such as upper band events.

We observe generally reduced occurrence rates of Moon-related wave events on field lines connected to magnetic anomalies. This is consistent with the reduced electron anisotropy by the magnetic mirror reflection as proposed by Harada et al. (2014). However, we pointed out the two notable exceptions. The first exception is the enhanced occurrence rate near latitudes from $-20°$ to $20°$ and longitudes from $-90°$ to $-60°$, where several isolated magnetic anomalies exist, including a strong magnetic anomaly called Reiner Gamma around latitude $8°$ and longitude $-58°$ (Kurata et al., 2005; Tsunakawa et al., 2015). This may imply that the spatial extent of the magnetic anomalies could play a role in the wave excitation, but it remains unclear why the magnetic connection to these isolated magnetic anomalies is favorable for the wave occurrence as opposed to spatially extended magnetic anomalies.

The second exception is the lower band only event on the night side of the solar wind and magnetosheath (Figures 7g and 8g). The occurrence rate distributions in these cases show no clear correlation with the magnetic anomalies, but rather show enhanced occurrence at certain latitude and longitude bands. This could result from sampling bias related to solar zenith angles as described in the following. For example, high latitude regions are biased toward solar zenith angles near $90°$. Similarly, because of tidal locking and the limited range of lunar phase in the solar wind, there are fewer observations at $0°$ longitude on the near side with solar zenith angles near $0°$ in the solar wind. This deviation of the solar zenith angle could affect the wave occurrence rate because of the gradual variation in the magnitude of the aforementioned electron anisotropy due to the transition of the lunar surface potential near the terminator (Halekas et al., 2008).

The relationship between the foot point solar zenith angle and the occurrence rates of Moon-related wave events is shown in Figure 11. For observations in the solar wind, magnetosheath, and magnetotail, the occurrence rates were calculated by dividing the number of identified events in each bin by the number of all observations in the bin, shown by the solid (dashed) magenta lines for unmagnetized (magnetized) regions. Here we categorize the unmagnetized (< 2 nT) and magnetized (>= 2 nT) regions according to the crustal field strength at the foot point longitude and latitude evaluated at a 30 km altitude by the lunar magnetic anomaly model of Tsunakawa et al. (2015). We only show the lower band only events, which have a relatively large number of events. The overall trend is that the occurrence rate is higher on the day side (at smaller solar zenith angles) and lower on the night side as already discussed. Additionally, the occurrence rates of both unmagnetized and magnetized regions decrease with increasing solar zenith angles on the night side in the solar wind and magnetosheath. The gradual decrease of the occurrence rates from 90° to 120° could explain the high-latitude enhancement of the occurrence rates seen in Figures 7g and 8g and the nearside enhancement in Figure 8g. In addition, the difference in occurrence rates between the unmagnetized and magnetized regions is smaller on the night side than on the day side. This could be because the electrostatic reflection from the negatively charged nightside surface occurs for both unmagnetized and magnetized regions, leading to relatively small differences in the effective electron anisotropy between the unmagnetized and magnetized regions.

Another notable signature is an enhancement of the occurrence rates near the terminator at 90° solar zenith angle in the magnetotail (Figure 11c). This could result from another sampling bias in the background plasma conditions. In the B_x (sunward/tailward component) dominant magnetotail lobes, the equatorial probe has a small chance of magnetic connection to the terminator during its orbit. Meanwhile, for more variable magnetic field directions in the plasma sheet, particularly during geomagnetically disturbed conditions, the probe has a higher probability of magnetic connection to the near-terminator surface. Consequently, the near-terminator foot point observations are disproportionately obtained in the plasma sheet, where intense, Moon-related whistler-mode waves are observed (Halekas, Poppe, Farrell, et al., 2012; Harada et al., 2014), possibly explaining the apparent increase of the near-terminator occurrence rates in the magnetotail.

5 Conclusions

In this study, we identified Moon-related whistler-mode waves from 9 years of ARTEMIS data and classified their spectral shapes in a fully automated manner, thereby statistically investigating the occurrence rates of four types of events: lower band only, upper band only, banded, and no-gap. The results are summarized as follows. (i) The occurrence rate of whistler-mode waves is enhanced over an order of magnitude on magnetic

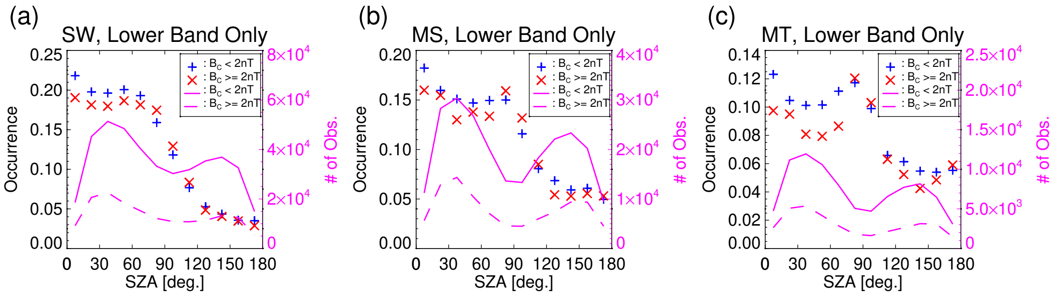

Figure 11. Occurrence rates of Moon-related lower band only wave events as functions of solar zenith angles observed in (a) the solar wind, (b) magnetosheath and (c) magnetotail; blue and red marks are for unmagnetized and magnetized regions. Solid (dashed) magenta lines show the number of all observations in each bin for unmagnetized (magnetized) regions.

field lines connected to the Moon (Moon-related wave events), indicating that the magnetic connection is a key factor for wave excitation. (ii) Banded events were rarely observed in the Moon-related wave events (occurrence ratios of banded/no-gap events <0.05 at the Moon as opposed to ∼2–3 in the terrestrial inner magnetosphere). (iii) The wave occurrence rate decreases when the magnetic field line is connected to the lunar night side compared to the day side, suggesting that the excitation of the whistler-mode waves is suppressed by lower anisotropy of upward traveling electrons resulting from the negative potential of the nightside lunar surface. (iv) The occurrence rate of the upper band waves is relatively low in the solar wind and magnetosheath in comparison to that in the magnetotail, suggesting that the excitation of high-frequency waves is suppressed by a lower temperature anisotropy of low-energy electrons in the plasma frame resulting from the moving obstacle effect. (v) The wave occurrence rates are generally decreased when the field line is connected to the lunar magnetic anomalies, which can be explained by lower anisotropy of electrons magnetically reflected from strong crustal magnetic fields as suggested by Harada et al. (2014), but we also identified exceptions of high occurrence rates near isolated, strong magnetic anomalies (e.g. Reiner Gamma).

The absence of banded events in the vicinity of the Moon makes a stark contrast to the common presence of a $0.5 f_{ce}$ gap for the chorus emissions in the terrestrial inner magnetosphere. These results suggest that the formation mechanisms for the two-band structure are much less effective in the lunar environment than those operating in the terrestrial inner magnetosphere. Specifically, we infer that the two-band structure formation by Landau damping or two electron components is not applicable to the near-Moon space given the plasma properties and magnetic field structure therein. Meanwhile, many of the detected wave amplitudes apparently exceed the wave-intensity threshold of the lower band cascade mechanism described in Gao et al. (2016), implying that some unidentified factors must be elucidated in order to account for the absence of banded events. It is notable that another characteristic signature of the chorus emissions, rising tone elements resulting from nonlinear growth, is present even around the Moon (Sawaguchi et al., 2021).

Additionally, we propose that the variability of wave spectral shapes arises from the varying shape of the electron velocity distribution function, which provides a free energy source for the excitation of whistler-mode waves. This variability can be caused by different degrees of deformation of electron velocity distributions by electrostatic and magnetic mirror reflections depending on the lunar surface charging, crustal magnetic field strength, and moving obstacle effect. Taken together, the presented results highlight the complexity and diversity of lunar plasma and electromagnetic environments, and reveal the similarities and differences between the lunar and terrestrial whistler-mode waves, thereby reinforcing the idea that the Moon provides a valuable natural plasma physics laboratory.

Acknowledgments

We acknowledge NASA contract NAS5-02099 and V. Angelopoulos for use of data from the THEMIS Mission. Specifically: O. LeContel and the late A. Roux for use of SCM data, and K. H. Glassmeier, U. Auster and W. Baumjohann for the use of FGM data provided under the lead of the Technical University of Braunschweig and with financial support through the German Ministry for Economy and Technology and the German Center for Aviation and Space (DLR) under contract 50 OC 0302. ARTEMIS data are publicly available at http://artemis.ssl.berkeley.edu.

References

Angelopoulos, V. (2011, DEC). The ARTEMIS mission. *Space Science Reviews*, *165*(1-4), 3-25. doi: 10.1007/s11214-010-9687-2

Auster, H. U., Glassmeier, K. H., Magnes, W., Aydogar, O., Baumjohann, W., Constantinescu, D., ... Wiedemann, M. (2008, DEC). The THEMIS Fluxgate Magnetometer. *Space Science Reviews*, *141*(1-4), 235-264. doi: 10.1007/s11214-008-9365-9

Burtis, W. J., & Helliwell, R. A. (1969). Banded chorus – A new type of VLF radiation observed in the magnetosphere by OGO 1 and OGO 3. *Journal of Geophysical Research*, *74*(11), 3002–3010. doi: 10.1029/JA074i011p03002

Burtis, W. J., & Helliwell, R. A. (1976). Magnetospheric chorus: Occurrence patterns and normalized frequency. *Planetary and Space Science*, *24*(11), 1007–1024. doi: 10.1016/0032-0633(76)90119-7

Coroniti, F. V., Scarf, F. L., Kennel, C. F., Kurth, W. S., & Gurnett, D. A. (1980). Detection of Jovian whistler mode chorus; Implications for the Io torus aurora. *Geophysical Research Letters*, *7*(1), 45–48. doi: 10.1029/GL007i001p00045

Cully, C. M., Angelopoulos, V., Auster, U., Bonnell, J., & Le Contel, O. (2011). Observational evidence of the generation mechanism for rising-tone chorus. *Geophysical Research Letters*, *38*(1). doi: 10.1029/2010GL045793

Fu, X., Cowee, M. M., Friedel, R. H., Funsten, H. O., Gary, S. P., Hospodarsky, G. B., ... Winske, D. (2014). Whistler anisotropy instabilities as the source of banded chorus: Van allen probes observations and particle-in-cell simulations. *Journal of Geophysical Research: Space Physics*, *119*(10), 8288-8298. Retrieved from `https://agupubs.onlinelibrary.wiley.com/doi/abs/10.1002/2014JA020364` doi: https://doi.org/10.1002/2014JA020364

Gao, X., Chen, L., Li, W., Lu, Q., & Wang, S. (2019). Statistical results of the power gap between lower-band and upper-band chorus waves. *Geophysical Research Letters*, *46*(8), 4098-4105. Retrieved from `https://agupubs.onlinelibrary.wiley.com/doi/abs/10.1029/2019GL082140` doi: https://doi.org/10.1029/2019GL082140

Gao, X., Lu, Q., Bortnik, J., Li, W., Chen, L., & Wang, S. (2016, MAR 28). Generation of multiband chorus by lower band cascade in the Earth's magnetosphere. *Geophysical Research Letters*, *43*(6), 2343-2350. doi: 10.1002/2016GL068313

Habagishi, T., Yagitani, S., & Omura, Y. (2014, JUN). Nonlinear damping of chorus emissions at local half cyclotron frequencies observed by GEOTAIL at L >9. *Journal of Geophysical Research: Space Physics*, *119*(6), 4475-4483. doi:

10.1002/2013JA019696

Halekas, J. S., Delory, G. T., Lin, R. P., Stubbs, T. J., & Farrell, W. M. (2008, SEP 4). Lunar prospector observations of the electrostatic potential of the lunar surface and its response to incident currents. *Journal of Geophysical Research-Space Physics*, *113*(A9). doi: 10.1029/2008JA013194

Halekas, J. S., Poppe, A., Delory, G. T., Farrell, W. M., & Horányi, M. (2012). Solar wind electron interaction with the dayside lunar surface and crustal magnetic fields: Evidence for precursor effects. *Earth, Planets and Space*, *64*(2), 3. doi: 10.5047/eps.2011.03.008

Halekas, J. S., Poppe, A. R., Farrell, W. M., Delory, G. T., Angelopoulos, V., McFadden, J. P., ... others (2012). Lunar precursor effects in the solar wind and terrestrial magnetosphere. *Journal of Geophysical Research: Space Physics*, *117*(A5). doi: 10.1029/2011JA017289

Harada, Y., Andersson, L., Fowler, C. M., Mitchell, D. L., Halekas, J. S., Mazelle, C., ... others (2016). MAVEN observations of electron-induced whistler mode waves in the Martian magnetosphere. *Journal of Geophysical Research: Space Physics*, *121*(10), 9717–9731. doi: 10.1002/2015GL067040

Harada, Y., & Halekas, J. S. (2016). Upstream waves and particles at the Moon. In Keiling, A and Lee, DH and Nakariakov, V (Ed.), *Low-Frequency Waves in Space Plasmas* (Vol. 216, p. 307-322).

Harada, Y., Halekas, J. S., Poppe, A. R., Kurita, S., & McFadden, J. P. (2014). Extended lunar precursor regions: Electron-wave interaction. *Journal of Geophysical Research: Space Physics*, *119*(11), 9160–9173. doi: 10.1002/2014JA020618

Harada, Y., Halekas, J. S., Poppe, A. R., Tsugawa, Y., Kurita, S., & McFadden, J. P. (2015, JUN). Statistical characterization of the foremoon particle and wave morphology: ARTEMIS observations. *Journal of Geophysical Research: Space Physics*, *120*(6), 4907-4921. doi: 10.1002/2015JA021211

Horne, R. B., Thorne, R. M., Shprits, Y. Y., Meredith, N. P., Glauert, S. A., Smith, A. J., ... Decreau, P. M. E. (2005, SEP 8). Wave acceleration of electrons in the Van Allen radiation belts. *Nature*, *437*(7056), 227-230. doi: 10.1038/nature03939

Hospodarsky, G. B., Averkamp, T. F., Kurth, W. S., Gurnett, D. A., Menietti,

J. D., Santolik, O., & Dougherty, M. K. (2008). Observations of chorus at Saturn using the Cassini Radio and Plasma Wave Science instrument. *Journal of Geophysical Research: Space Physics*, *113*(A12). doi: 10.1029/2008JA013237

Katoh, Y., & Omura, Y. (2011). Amplitude dependence of frequency sweep rates of whistler mode chorus emissions. *Journal of Geophysical Research: Space Physics*, *116*(A7). doi: 10.1029/2011JA016496

Kennel, C. F., & Petschek, H. E. (1966). Limit on stably trapped particle fluxes. *Journal of Geophysical Research*, *71*(1), 1–28. doi: 10.1029/JZ071i001p00001

Khabibrakhmanov, I., & Summers, D. (1997, APR 1). On the theory of Alfven waves in the solar wind. *Journal of Geophysical Research: Space Physics*, *102*(A4), 7095-7104. doi: 10.1029/96JA03843

Kurata, M., Tsunakawa, H., Saito, Y., Shibuya, H., Matsushima, M., & Shimizu, H. (2005, DEC 28). Mini-magnetosphere over the Reiner Gamma magnetic anomaly region on the Moon. *Geophysical Research Letters*, *32*(24). doi: 10.1029/2005GL024097

Kurita, S., Katoh, Y., Omura, Y., Angelopoulos, V., Cully, C. M., Le Contel, O., & Misawa, H. (2012). THEMIS observation of chorus elements without a gap at half the gyrofrequency. *Journal of Geophysical Research: Space Physics*, *117*(A11). doi: 10.1029/2012JA018076

Menietti, J. D., Horne, R. B., Gurnett, D. A., Hospodarsky, G. B., Piker, C. W., & Groene, J. B. (2008). A survey of Galileo plasma wave instrument observations of Jovian whistler-mode chorus. *Annales Geophysicae*, *26*(7), 1819–1828. Retrieved from `https://www.ann-geophys.net/26/1819/2008/` doi: 10.5194/angeo-26-1819-2008

Menietti, J. D., Santolik, O., Rymer, A. M., Hospodarsky, G. B., Gurnett, D. A., & Coates, A. J. (2008). Analysis of plasma waves observed in the inner Saturn magnetosphere. In *Annales Geophysicae: Atmospheres, Hydrospheres and Space Sciences* (Vol. 26, p. 2631). doi: 10.1029/2007JA012856

Omura, Y. (2021, APR 20). Nonlinear wave growth theory of whistler-mode chorus and hiss emissions in the magnetosphere. *Earth, Planets and Space*, *73*(1). doi: 10.1186/s40623-021-01380-w

Omura, Y., Hikishima, M., Katoh, Y., Summers, D., & Yagitani, S. (2009, JUL 18). Nonlinear mechanisms of lower-band and upper-band VLF chorus emissions in the magnetosphere. *Journal of Geophysical Research: Space Physics*, *114*. doi: 10.1029/2009JA014206

Omura, Y., Katoh, Y., & Summers, D. (2008). Theory and simulation of the generation of whistler-mode chorus. *Journal of Geophysical Research: Space Physics*, *113*(A4). doi: 10.1029/2007JA012622

Poppe, A. R., Farrell, W. M., & Halekas, J. S. (2018). Formation timescales of amorphous rims on lunar grains derived from artemis observations. *Journal of Geophysical Research: Planets*, *123*(1), 37-46. Retrieved from `https://agupubs.onlinelibrary.wiley.com/doi/abs/10.1002/2017JE005426` doi: 10.1002/2017JE005426

Roux, A., Le Contel, O., Coillot, C., Bouabdellah, A., de la Porte, B., Alison, D., … Vassal, M. C. (2008, DEC). The Search Coil Magnetometer for THEMIS. *Space Science Reviews*, *141*(1-4), 265-275. doi: 10.1007/s11214-008-9455-8

Sawaguchi, W., Harada, Y., & Kurita, S. (2021, JAN 16). Discrete rising tone elements of whistler-mode waves in the vicinity of the Moon: ARTEMIS observations. *Geophysical Research Letters*, *48*(1). doi: 10.1029/2020GL091100

Scarf, F. L., Gurnett, D. A., & Kurth, W. S. (1981). Measurements of plasma wave spectra in Jupiter's magnetosphere. *Journal of Geophysical Research: Space Physics*, *86*(A10), 8181-8198. Retrieved from `https://agupubs.onlinelibrary.wiley.com/doi/abs/10.1029/JA086iA10p08181` doi: 10.1029/JA086iA10p08181

Shue, J. H., Chao, J. K., Fu, H. C., Russell, C. T., Song, P., Khurana, K. K., & Singer, H. J. (1997, MAY 1). A new functional form to study the solar wind control of the magnetopause size and shape. *Journal of Geophysical Research: Space Physics*, *102*(A5), 9497-9511. doi: 10.1029/97JA00196

Smith, E. J., & Tsurutani, B. T. (1976). Magnetosheath lion roars. *Journal of Geophysical Research: Space Physics*, *81*(13), 2261-2266. doi: 10.1029/JA081i013p02261

Teng, S., Tao, X., & Li, W. (2019, APR 16). Typical characteristics of whistler mode waves categorized by their spectral properties using Van Allen Probes observations. *Geophysical Research Letters*, *46*(7), 3607-3614. doi: 10.1029/2019GL082161

Thorne, R. M., Li, W., Ni, B., Ma, Q., Bortnik, J., Chen, L., … Kanekal, S. G.

(2013, DEC 19). Rapid local acceleration of relativistic radiation-belt electrons by magnetospheric chorus. *Nature*, *504*(7480), 411+. doi: 10.1038/nature12889

Tsunakawa, H., Takahashi, F., Shimizu, H., Shibuya, H., & Matsushima, M. (2015, JUN). Surface vector mapping of magnetic anomalies over the Moon using Kaguya and Lunar Prospector observations. *Journal of Geophysical Research: Planets*, *120*(6), 1160-1185. doi: 10.1002/2014JE004785

Tsurutani, B. T., & Smith, E. J. (1974). Postmidnight chorus: A substorm phenomenon. *Journal of Geophysical Research*, *79*(1), 118–127. doi: 10.1029/JA079i001p00118

Tsurutani, B. T., Smith, E. J., Anderson, R. R., Ogilvie, K. W., Scudder, J. D., Baker, D. N., & Bame, S. J. (1982). Lion roars and nonoscillatory drift mirror waves in the magnetosheath. *Journal of Geophysical Research: Space Physics*, *87*(NA8), 6060-6072. doi: 10.1029/JA087iA08p06060

Whipple, E. C. (1981). Potentials of surfaces in space. *Reports on Progress in Physics*, *44*(11), 1197-1250. doi: 10.1088/0034-4885/44/11/002

Supporting Information for "Spectral properties of whistler-mode waves in the vicinity of the Moon: A statistical study with ARTEMIS"

W. Sawaguchi[1], Y. Harada[1], S. Kurita[2]and S. Nakamura[3]

[1]Department of Geophysics, Graduate School of Science, Kyoto University, Kyoto, Japan.

[2]Research Institute for Sustainable Humanosphere, Kyoto University, Uji, Japan.

[3]Institute for Space-Earth Environmental Research, Nagoya University, Nagoya, Japan.

Contents of this file

Introduction

The supporting materials are consist of a table and text describing the table. The table shows the result of an algorithm test.

Text S1.

We tested the algorithm used in our study by applying it to the Time History of Events and Macroscale Interactions during Substorms (THEMIS) SCM onboard FFT spectra, which are equivalent to the ARTEMIS data used in the manuscript. Here the data are obtained by THEMIS D and E from Apr. 24, 2010 to Mar. 21, 2011 when the FFT spectra were obtained in a 64-bin resolution. On applying them to Earth's inner magnetosphere, we slightly changed the criteria from the lunar analysis presented in the paper. The threshold power spectral density for event identification is changed to $p_{th} = 10^{-7}$ nT^2/Hz (an order of magnitude larger than in Teng et al. (2019)) to take into account the relatively small noise floor at a frequency range of whistler-mode wave generation in the inner magnetosphere. In addition, following Teng et al. (2019), observations in the plasmasphere are excluded with a condition that the number density of electrons exceeds 100 cm^{-3}. The result is shown in Table S1. We note that the ratio of lower band only events is far larger than that of Teng et al. (2019). This may be because the relatively large p_{th} compared to Teng et al. (2019) results in underestimation of typically weak upper band waves (Gao et al., 2019). One another possibility comes from the difference that we did not visually checked the events and therefore some other events may be included such as hiss emissions. In any case, the ratio of banded to no-gap is approximately 2, generally reproducing the results of Teng et al. (2019) ($\sim$ 3) and Gao et al. (2019) ($\sim$ 2). Hence, we conclude that the algorithm and FFT spectra of THEMIS-ARTEMIS are sufficient for distinguishing the gap of whistler-mode waves.

Table S1. Number (ratio) of four types of whistler-mode events observed by THEMIS.

Lower	Upper	Banded	No-gap
500,711 (93.0%)	11,840 (2.2%)	17,567 (3.3%)	8,570 (1.6%)